Lavallée, D., S. Lovejoy, D. Schertzer, P. Ladoy, 1993: Nonlinear variability and Landscape topography: analysis and simulation. **Fractals in Geography**, Eds. L. De Cola, N. Lam, 158-192, PTR, Prentice Hall.

CHAPTER 8

NONLINEAR VARIABILITY OF LANDSCAPE TOPOGRAPHY: MULTIFRACTAL ANALYSIS AND SIMULATION

Daniel Lavallée
Earth Science Research Group, University of California, Santa Barbara

Shaun Lovejoy
Physics Department, McGill University, Montreal, Canada

Daniel Schertzer
Laboratoire de Météorologie Dynamique, Université Pierre et Marie Curie, Paris, France

Philippe Ladoy
Météorologie Nationale, Paris, France

ABSTRACT

We argue that geographic and geophysical fields are generally multifractal (characterized by an infinite hierarchy of fractal dimensions) and that inconsistencies are inevitable when they are forced into narrow geometric frameworks involving single fractal dimensions. As an example, we show how commonly used monofractal relationships between fractal dimensions and spectral and variogram exponents break down for multifractals. We then review some results on multifractal processes showing how they lead to universal multifractals with generators characterized by the three basic parameters H, C_1, and α. The parameter H measures the degree of nonstationarity of the process, C_1 is the codimension that characterizes the sparseness–inhomogeneity of the mean of the process, and α characterizes the degree of multifractality; $\alpha = 0$ is monofractal, $\alpha = 2$ is the maximum.

We then describe a new Double Trace Moments (DTM) technique, which is the first data-analysis technique specifically designed to estimate these parameters. We apply the technique to digital elevation maps of Deadman's Butte (50-m resolution) and French topography (1-km resolution), finding roughly compatible estimates of the multifractal index $\alpha = 1.9 \pm 0.1$ and 1.7 ± 0.1, respectively (close to its maximum). Interestingly, $C_1 \approx 0.045 \pm 0.005$ and $C_1 \approx 0.075 \pm 0.005$, respectively, which indicate that the mean of the process is not far from the space-filling value 0. We also find $H \approx 1/2$, and we use dimensional analysis to suggest possible physical explanations. The low values of C_1 show why monofractal models such as fractional Brownian motion may give reasonable results for the mean of the topography, but are poor models for the extremes; multifractal effects (that is, large sparse fluctuations) become important rapidly for high-order moments and for regions at very high (or very low) altitudes. Finally, we produce simulations of topography with the observed multifractal parameters.

INTRODUCTION

Scale Invariance and Nonlinear Variability of Geographical Data

Geophysical and geographical systems are characterized by extreme spatial and temporal variability, fractal structures spanning wide ranges of scale, and nonlinear dynamics. This ubiquitous nonlinear variability is increasingly being recognized as a central geophysical and geographical problem (see, for example, the preface and various contributions to Schertzer and Lovejoy, 1991a). The explosion of interest in chaos, fractals, and scaling, and, more recently, multifractals and multiscaling, has led to rapid advances in understanding this variability. The most promising of the new developments for geophysics and geography has undoubtedly been in scaling ideas that are now helping to provide a unified picture of atmospheric and other geophysical systems. Indeed, for some time we have proposed that scale invariance is a symmetry principle capable of unifying the earth sciences.

Unfortunately, the current honeymoon between scaling and geophysics has been dominated by restrictive monofractal ideas associated with fractal sets and the obsession with unique scaling exponents (especially the fractal dimension). Furthermore, only very special types of scale-changing operations have been considered; only self-similar or occasionally self-affine transformations have been employed. In the former case, the small scales are reduced carbon copies of the large, and in the latter case, "squashing" or "compression" along coordinate axes is also permitted. With the development of multifractals and generalized scale invariance (GSI) (Schertzer and Lovejoy, 1983, 1985), it is now clear that the types of scaling can be much broader. In particular, scale-invariant systems can now include fields rather than sets (that is, multifractal measures), and the types of possible scale transformations encompass not only differential stratification (self-affinity) but also rotation and anisotropy which varies from one place to another. A further step away from geometry toward a dynamical formalism of scale invariance was the recognition that multifractals possess stable and attractive universal generators (Schertzer and Lovejoy, 1987, 1989a, 1989b; Schertzer et al., 1988, 1991). This greatly simplifies the analysis and modeling of multifractals by replacing the infinite number of multifractal

exponents by a small number of dynamically significant parameters. In the following, we illustrate some of these ideas by estimating the fundamental multifractal index α using a digital elevation model and a new data analysis technique called *double trace moments* (DTM) (Lavallée, 1991). We then use the estimated parameters to produce multifractal simulations of topography. Our results help explain both the successes and limitations of the monofractal models: although we find a nearly maximum degree of multifractality, the mean of the process is not very sparse; hence multifractal effects will not be too noticeable for low-order statistics; they will, however, dominate the behavior of the extremes, such as the high-order moments or very high/low-altitude regions.

Scaling, Fractals, and Topography

The problem of adequately conceptualizing and representing the earth's topography (for example, coastlines and rivers) has a long history. It includes Perrin's (1913) discussion of the "tangentless" coastline of Brittany and Steinhaus's (1954) discussion of the nonrectifiable nature of rivers.[1] The scaling nature of the topography has also been known for some time. In a paper entitled "A Remarkable Feature of the Earth's Topography," Venig-Meinesz (1951) found a power-law spectrum over wide ranges and correctly recognized its fundamental significance. Bell (1975) showed that Venig-Meinisz's spectral scaling of the altitude of the topography extends from planetary scales at least down to 0.15 km; using satellite data, Bills and Kobrick (1985) showed that Venus, Mars, and the moon have very similar scaling exponents to the earth. Similarly, using yardsticks of varying lengths, Richardson (1961) found various coastlines to be scaling over wide ranges and determined the relevant exponents. Mandelbrot (1967) related Richardson's exponents to fractal dimensions.

A new impetus for fractal analyses of topography came from fractional Brownian motion models of terrain (Mandelbrot 1975, 1977; Voss, 1983; Fournier et al., 1982; Clarke, 1988), which produced strikingly realistic looking models of mountains. However, in spite of the now mushrooming interest in the field, direct estimates of fractal dimensions of various topographic sets (for example, lines of constant altitude) have not been numerous. The main examples of which we are aware are Goodchild (1980), Aviles et al. (1987), Okubo and Aki (1987), and Turcotte (1989) (who also pointed out some apparent contradictions in the monofractal analyses).[2] See also Klinkenberg and Goodchild (1992) and Klinkenberg and Clarke (1992) for reviews and discussions. Other relevant direct

[1] "...The left bank of the Vistula, when measured with increased precision would furnish lengths ten, hundred, and even a thousand times as great as the length read off a school map. A statement nearly adequate to reality would be to call most arcs encountered in nature not rectifiable. This statement is contrary to the belief that not rectifiable arcs are an invention of mathematicians and that natural arcs are rectifiable: it is the opposite that is true..." (Steinhaus, 1954). In a popular book (Steinhaus, 1962), the argument is repeated and as an illustration of the point, a (fractal) Peano curve is shown.

[2] We specifically exclude variogram methods such as those reported in Mark and Aronson (1984) and Rees and Muller (1990) or spectral exponent methods such as those reported in Gilbert (1989) and Mareschal (1989), since both methods measure different scaling exponents, neither of which are fractal dimensions. They could have been used to infer fractal dimensions only if the topography had been monofractal rather than multifractal.

empirical estimates of fractal dimensions of surface features are given in De Cola (1989, 1990) (the former also includes a short discussion of multifractals). The multifractal analyses of topography are more recent and are found in Ladoy et al. (1990) and Lovejoy and Schertzer (1990a), and the corresponding multifractal simulation studies are in Wilson et al. (1991) and Sarma et al. (1990) (see Figures 8.1a and b and 8.2a and b). Other relevant empirical multifractal analyses in geophysics are the rainfield, clouds, wind and temperature, networks, and rain measurement (Lovejoy et al., 1987; Tessier et al., 1993; Schmitt et al., 1992a, b; Gabriel et al., 1988). For reviews, see Lovejoy and Schertzer (1988a, b, 1990b, 1991) and Schertzer and Lovejoy (1988, 1989a, b). Below, we show how a new multifractal analysis technique called the double trace moment (the DTM technique), when carefully applied to topographic data, enables us to estimate directly the fundamental universal multifractal parameters of topography.

Multifractals: Beyond the Geometry of Sets

A fractal is a geometrical set of points; a multifractal is a mathematical measure. When integrated–averaged over a resolution scale, this will be a field with intensity values

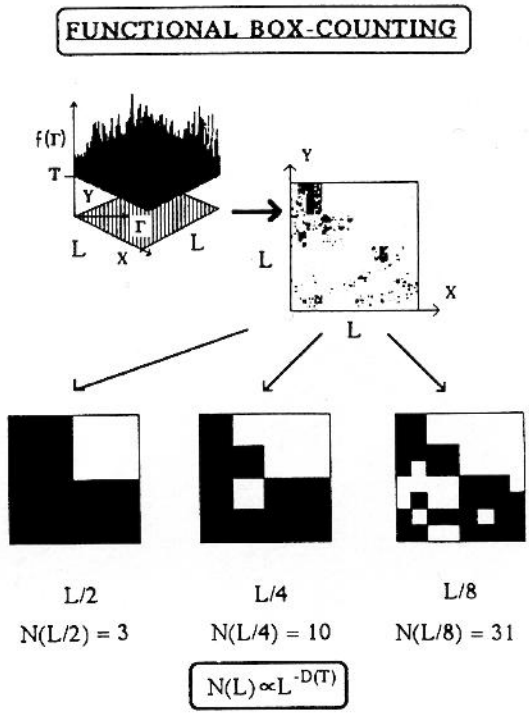

Figure 8.1(a) Schema showing how functional box counting can be used to estimate the fractal dimensions at various thresholds T.

defined everywhere. In geophysics and often in geography, we are rarely directly interested in sets of points. Indeed, a significant part of a map maker's skill is to find an adequate way of representing various fields such as population density, altitude, depth of ocean, temperature, and so on. To obtain sets, we typically establish thresholds and define the set of interest (for example, an *exceedance* set) to comprise all the points above a threshold, delineating them with *isolines*. Closer inspection shows that the relationship between the real world and various cartographic sets is rather indirect: the remote sensor has an intrinsic spatial–temporal resolution typically much larger than the smallest scale of the phenomenon we seek to represent. Therefore, the very first step of analysis, as we impose an inner scale to obtain a finite resolution *field* (pixel world), already involves a fundamental symmetry breaking through averaging, smoothing, or sampling (Schertzer and Lovejoy, 1991b). On the contrary, most geographers and geophysicists have forgotten this important first step, and the monofractal approach exemplified by Mandelbrot (1982) remains the general approach (see the special issue of *Pure and Applied Geophysics* on fractals in *Physics*, Vol. 132, 1989). They have taken for granted the representation of nature by geometrical fractal sets and by various mathematical functions that yield fractal sets in simple ways (for example, the exceedance sets mentioned above). In contrast, the study of nonlinear variability (in particular, that arising in turbulent cascade processes) has shown that scaling processes generically give rise to multifractal measures with very singular small-scale limits; many results derived for fractal sets and monofractal functions will not apply (This is much more fundamental than the problems discussed by Fox, 1989).

The reason that the initial averaging, smoothing, or sampling operation is a nontrivial step is that multifractals are not defined point by point, but rather they are defined on small neighborhoods of points (that is, they are nonlocal). Furthermore, they are also statistical; their variability can be "hard" in the sense that the spatial–temporal averaging

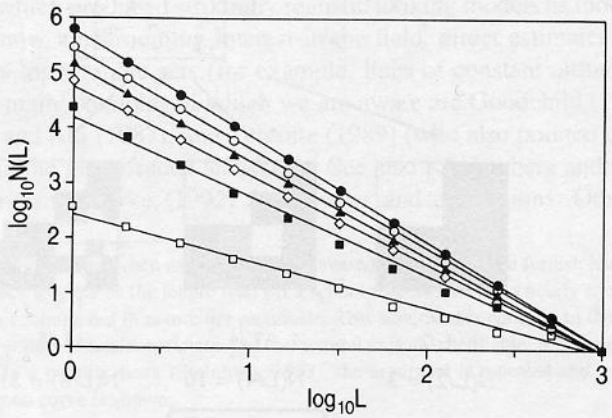

Figure 8.1(b) The results of functional box counting when applied to 1024 × 1024km topographic map of France at 1-km resolution. The lines (bottom to top) are the box-counting results for altitude thresholds decreasing by factors of 2 from 3600 m above sea level. The corresponding dimensions increase from 0.84 (at 3600 m) to 1.92 (at 28 m) (From Lovejoy and Schertzer, 1990a).

may not be enough to tame (that is, smooth out) some of the more violent fluctuations (leading for example to the phenomenon of divergence of high-order statistical moments; the "hard" behavior discussed in Schertzer and Lovejoy, 1992). Limiting our attention to fractal sets and monofractal analysis techniques is partly a result of the over emphasis on geometry at the expense of the more abstract but more powerful statistical notions of scale

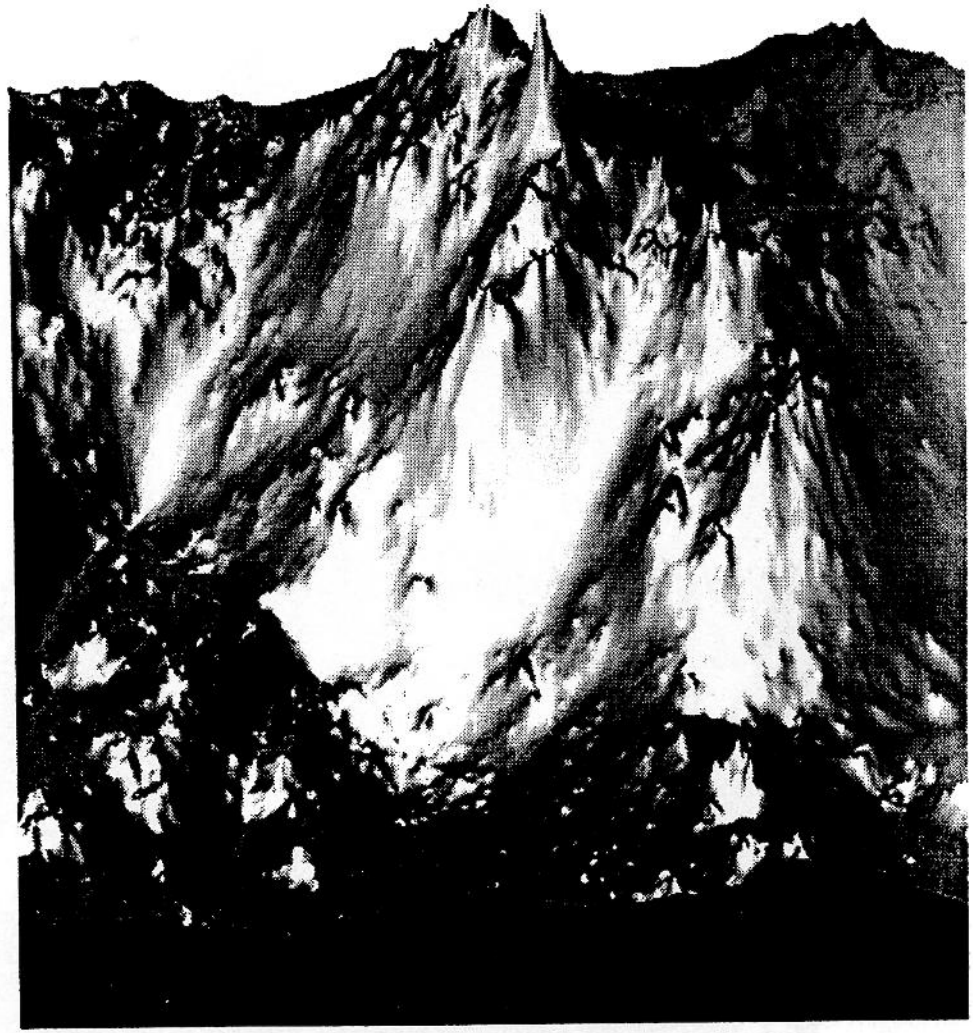

Figure 8.2(a) This figure and the next illustrate the zooming technique applied in the case of the continuous multiplicative cascade with Gaussian generator ($\alpha = 2$ and $C_1 = 0.5$). The 256×256 window, chosen exactly in the center of this 512×512 resolution image, is zoomed by a factor of 2 in Figure 8.2b. The insertion of small-scale detail is done in a multiplicative way by developing the cascade processes to the appropriate scale length. These figures are reproduced from Wilson, et al., 1991.

invariance needed to deal with multifractals. Specifically, it has led to frustrating attempts to square simplistic monofractal analysis methods with multifractal data. In the following, using an example of topographic data, we wish to clear up some of these issues and show how multifractals can explain some of the apparently contradictory results reported in the literature.

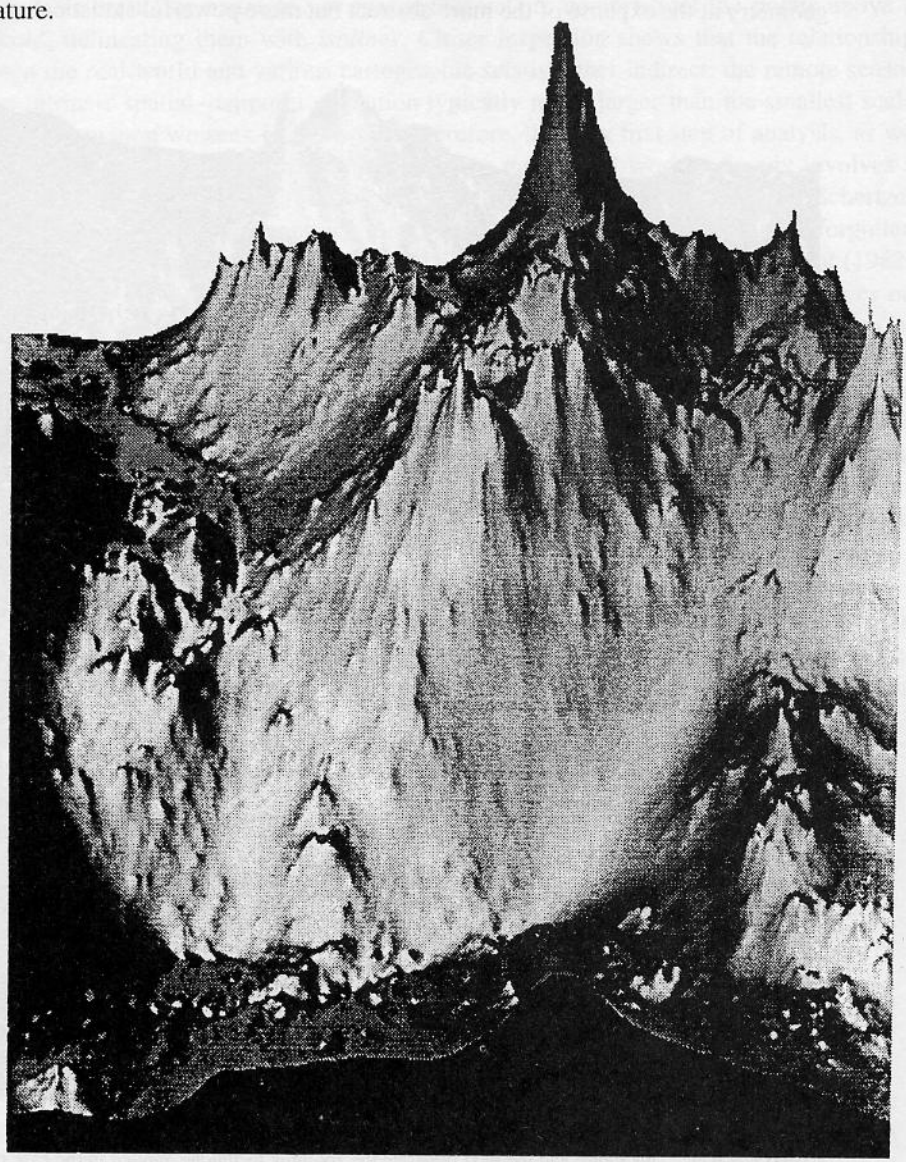

Figure 8.2(b) The resulting images where the large structures are well reproduced (for example, the sharp peak in the center), but new small-scale details have appeared, characterized by the same universal scaling parameters.

FRACTAL SETS, MONOFRACTAL FUNCTIONS, AND MULTIFRACTALS

Fractal Sets, Dimensions, and Codimensions

The simplest illustration of scaling and scale invariance is to consider the dimension of a set of points (S). The intuitive definition is that the *contents* (or "volume") of the set $n(l)$ at scale l is given by

$$n(l) \propto l^{D(S)} \tag{8.1}$$

where $D(S)$ is the dimension (for example, the length, or the "volume," of a line $\propto l$, the area of a plane $\propto l^2$, and so on). The volume (that is, the measure of the set) is therefore a simple scaling (power law) function, and the dimension is important precisely because it is scale invariant (independent of l) (See Lovejoy et al., 1986a, b for the example of geophysical measuring networks). Alternatively, rather than looking at larger regions of the set [as in $n(l)$], we may consider $N(l)$, the number of boxes of size l, needed to cover it. The covering could be regarded as a spatially degraded version of the original set of scale l. Since the number of points of S covered by each box is $n(l)$, we clearly have $N(l)n(l) \approx$ constant; hence $N(l) \propto l^{-D(S)}$. The $D(S)$ obtained by this box-counting procedure can be considered as an *estimate* of the Hausdorff dimension of the set; it is also called the fractal dimension, box-counting dimension, and, earlier, capacity dimension (Kolmogorov and Tihomirov, 1959). In practice, the Hausorff dimension is often too difficult to deal with directly, even for sets studied by mathematicians. In physical applications, the primary complications that can arise if box-counting dimensions are used as approximations to Hausdorff dimensions are various log-corrections in $N(l)$. However, in specially concocted mathematical sets, significantly different dimensions can be obtained; see Falconer (1990) for a discussion.

Although a given set may be fractal, we are usually more interested in its distribution, which is generally multifractal and involves codimensions rather than dimensions. The codimension $C(S)$ of S is the scaling exponent of the fraction of the space occupied by the set, which is also equal to the probability $P(l)$ of finding the set in a given l sized box:

$$P(l) \propto l^{C(S)} \tag{8.2}$$

Since $C(S)$ determines the scaling of the probability, it is a statistical exponent that is defined *intrinsically*. This means that it is determined by the underlying (usually stochastic) generating process and requires no reference to the dimension of the space on which it is observed. In contrast, the fractal dimension depends on the intersection of the process with an observing space of dimension D, where $N(l)$ is given by the probability $P(l)$ multiplied by the total number of boxes on the observing set l^{-D}. Hence, if the observing set has a large enough dimension [$D > C(S)$] for intersection to occur (and hence for observation to be possible), then $D(S) = D - C(S)$. Since we will be generally interested in stochastic processes defined on probability spaces with infinite dimension ($D \rightarrow \infty$), the use of codimensions (which will still be finite and still characterize the sparseness of the probability space) is obligatory. The use of codimensions avoids the paradoxes of *latent* (that is, nega-

tive) fractal dimensions arising when a multifractal process is studied on low-dimensional cuts with $D < C(S)$.

Monofractal Functions, Exceedance Sets, and Isolines

Since geographers and geophysicists are interested in fields, models for scaling phenomena have usually involved scaling functions. When the latter are linear (for example, produced by summing either correlated or independent random noises), then the functions produced can generally be characterized by a single scaling exponent, and the associated sets will have unique fractal dimensions. In contrast, multifractals are produced by the (nonlinear) multiplication of elementary random noises and involve multiple scaling exponents and multiple fractal dimensions. Furthermore, they are generally not defined at mathematical points; they are not functions but rather measures. Below, we first discuss monofractal functions emphasizing their limitations.

Consider the function $h(\underline{x})$, which represents the height at a point $\underline{x}$. In this subsection, we consider the special case where h is a random scaling function with the following properties:

$$\Delta h_{l/\lambda} \stackrel{d}{=} \lambda^{-H} \Delta h_l \tag{8.3}$$

where the small-scale altitude difference is $\Delta h_{l/\lambda} = h(\underline{x}_1 + \lambda^{-1}\,\Delta\underline{x}) - h(\underline{x}_1)$ and the large-scale difference is $\Delta h_l = h(\underline{x}_2 + \Delta x) - h(\underline{x}_2)$ where $\underline{x}_1$, $\underline{x}_2$ are arbitrary, $\lambda(>1)$ is a reduction ratio, $l = |\Delta\underline{x}|$ is the separation distance, and H is the unique scaling parameter that characterizes the degree of nonstationarity of the topography. The equality $\stackrel{d}{=}$ means equality in probability distributions, $a \stackrel{d}{=} b$ if and only if $\Pr(a > q) = \Pr(b > q)$ for all q, where Pr indicates probability. This type of simple scaling[3] could also be called *scaling of the increments*. A special case in which the probability distributions of the altitude increments Δh are Gaussian is called *fractional Brownian motion* and can be obtained, for example, by passing Gaussian white noise through a power-law filter (that is, by fractional integration; normal Brownian motion is obtained by the usual nonfractional integration). This notion was introduced by Kolmogorov (1940); the expression was coined by Mandelbrot and Van Ness (1968); these are the very special processes used to make the now familiar monofractal mountains.

Given a function $h(\underline{x})$, sets can be defined in many different ways. First, consider the exceedance set $S_{\geq T}$ as the set of all points x satisfying $h(x) \geq T$ (that is, those regions whose altitude equals or exceeds the threshold T). In general, if $T_1 > T_2$, then $S_{\geq T1}$ will be a subset of $S_{\geq T2}$ and hence $D(S_{\geq T1}) \leq D(S_{\geq T2})$ (see Figures 8.1a and b for empirical confirmation of this multifractal behavior). However, for the special case of simple scaling, $S_{\geq T}$ will not be a fractal set al all, and $D(S_{\geq T}) = D$ irrespective of T. Similarly, the *graph of* h, G, is defined as the set of points $(x, h(x))$ in a $(D + 1)$-dimensional space, for example, when $D = 2$, on a

[3]This type of scaling was first introduced by Lamperti (1962) under the name "semistable." It was called "self-similarity" by Mandelbrot and Van Ness (1968). However, this name turned out to be a misnomer since the actual functions f were not self-similar but self-affine, and self similarity is a much wider concept anyway.

topographic surface. Again, in the special case of simple scaling, there is a unique codimension (and dimension) associated with G, where $C(G) = H$, and we obtain the well-known result $D(G) = 3 - H$ for Voss's (1983) and Mandelbrot's (1982) celebrated monofractal landscapes.

We can also define the *perimeter set* P_T associated with $S_{\geq T}$. P_T is the *border* set of $S_{\geq T}$ defined as the *level set* or *T-crossing set* of G with the plane $h(\underline{x}) = T$. It is the set of points such that arbitrarily small neighborhoods of $\underline{x}$ contain some points with $h(\underline{x}) < T$ and some such that $h(\underline{x}) \geq T$. $D(P_T)$ will be the dimension of the isolines on a topographic map of $h(\underline{x})$. By definition P_T is a subset of $S_{\geq T}$; hence $D(P_T) \leq D(S_{\geq T})$. In general, it will depend on the connectedness properties of $S_{\geq T}$ and increase or decrease with T only being bounded above by the decreasing function $D(S_{\geq T})$. Finally, we may define $S_{=T}$ as the set of points x such that $h(\underline{x}) = T$. Clearly, it will be a subset of P_T; hence generally, $D(P_T) \geq D(S_{=T})$. However, in simple scaling we obtain the simple result $C(P_T) = C(S_{=T}) = H$; hence isolines in simple scaling models of topography will have dimensions $D(P_T) = D(S_{=T}) = 2 - H$ independent of T.

Variograms, Spectra, and the Distribution of Islands

The relationship $C(P_T) = H$ combined with Equation 8.1 has led to a popular way of estimating $D(P_T)$. By taking qth powers of the modulus of both sides of Equation 8.3 and taking ensemble (that is, statistical) averages (indicated by $< >$), we obtain

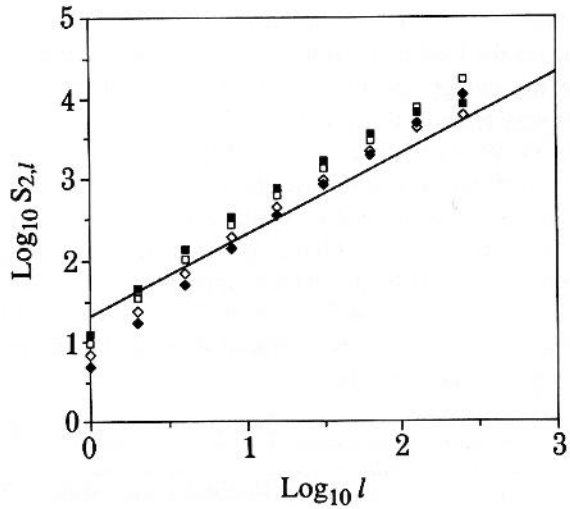

Figure 8.3 First- and second-order structure functions or variograms of the Deadman's Butte data, in both east–west (x) and north–south (y) directions, are shown along with a reference line of slope = 1 (corresponding to a spectral exponent of $\beta = 2$). The functions $S_2(\Delta x)$, $(S_1(\Delta x))^2$, $S_2(\Delta y)$, and $(S_1(\Delta y))^2$ are shown, respectively, by white squares, black diamonds, black squares, and white diamonds.

$$S_{q,l} = \langle |\Delta h_l|^q \rangle$$

$$S_{q,l/\lambda} = \lambda^{K_h(q)} S_{q,l} \tag{8.4}$$

where $K_h(q)$ is the scaling exponent of the qth-order structure function $S_{q,l}$ (also called *variogram* when $q = 2$). In the special case of simple scaling, $K_h(q)$ is linear: $K_h(q) = -Hq$; in multifractals, it will be convex (nonlinear). Unfortunately, the linearity of $K_h(q)$ is usually simply assumed and H is estimated as $K_h(2)/2$. The relation $H = C(P_T)$ is then used to estimate the fractal dimension of the isolines and graph. For an example on topography, Figure 8.3 shows the results for the Deadman's Butte digital elevation map (50-m resolution, 512 × 512 points). We already can see (Figure 8.4) that $K_h(2) \neq 2K_h(1)$; discussion of this multiple scaling is given in the following section. It involves convex functions $K_h(q)$, and exceedance sets $S_{\geq T}$ will have fractal dimensions that decrease as the threshold is increased.

Now consider the energy spectrum $E(k)$ of scaling processes.[4] Irrespective of whether or not there is simple or multiple scaling, we will have $E(k) = k^{-\beta}$, where k is the wave number. (This ignores possible log corrections or effects of anisotropic scale invariance.) This type of spectrum is relevant for the problem of surface topography since it has been known for some time (Venig-Meinesz, 1951) that $\beta \approx 2$ for the earth. Bills and Kobrick (1985) show that this behavior holds for at least five orders of magnitude in scale (from planetary scales down to at least ≈0.15 km). Figure 8.5 illustrates that it is also roughly true for the Deadman's Butte data analyzed here where we obtained $\beta \approx 1.93$.

Since the energy spectrum is the Fourier transform of a second-order moment ($q = 2$), it is easy to show that $\beta = 1 - K_h(2)$. For example, with the Deadman's Butte data (Figure 8.3a and b), we have $K_h(2) = -1.1 \pm 0.2$, $\beta = 1.93 \pm 0.03$. In the case of simple scaling, $K_h(2) = -2H$; we therefore have the two special relations $\beta = 1 + 2H = 1 + 2C(P_T)$. These relations have been widely popularized for the case of lines embedded in planes ($D = 2$), surfaces embedded in volumes ($D = 3$) in the form $D(P_T) = (5 - \beta)/2$, $D(P_T) = (7 - \beta)/2$ respectively. Since in virtually all these applications, the lines or surfaces are likely to be multifractals, these relations will not hold. This means that there is not necessarily any contradiction between estimates of fractal dimensions of lines of constant altitude and spectral or variogram exponents.

[4]In Fourier space, the dilation (magnification) $x \rightarrow \lambda x$ is equivalent to $k \rightarrow \lambda^{-1}k$. In spaces dimension 2 and higher, more general anisotropic dilations (generalized scale invariance) are required. These will give rise to the appearance of texture, which will generally give logarithmically periodic modulations of the spectra about the simple power law given here (see Pflug et al., 1993 for more details and an application to cloud texture). This could explain the small discrepancy in power law topography spectra reported by Gilbert (1989). Probably the most significant source of deviation from the expected power laws followed in the latter's spectra are due to small sample sizes, (usually, the spectrum of a single realization is used), not the ensemble averages. For precise estimates of the necessary size (the *sampling dimension*), see Lavallée et al., 1991.

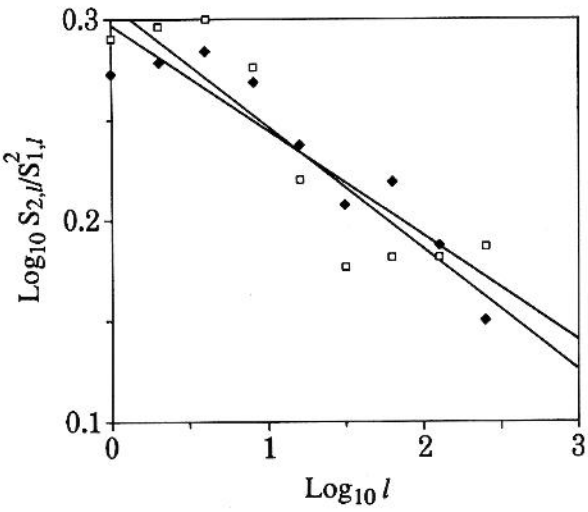

Figure 8.4 We show the log ratios of log $(S_2(\Delta x)/(S_1(\Delta x))^2)$ and log $(S_2(\Delta y)/(S_1(\Delta y))^2)$ as functions of the log lags, along with their best fit slopes, which are estimates of $K_h(2) - 2K_h(1) \approx C_1$ (see text). Although the method is not accurate due to the small sample size, the slopes are 0.055 and 0.065, which are consistent with the C_1 estimated below.

Finally, we may consider the number of simply connected areas (*islands*) that exceed the threshold T. Due to the scale invariance, we may expect the following power-law distribution:

$$Nr\,(A_T > a_T) = a_T^{-B_T}, \quad a_T >> 1 \tag{8.5}$$

where Nr indicates the number of islands defined by the threshold T whose area A_T exceeds a fixed threshold a_T. For the earth, when T is taken as sea level, the simply connected regions are true islands; B_T has been estimated by Korcak (1938) as $B_T \approx 0.8$. Mandelbrot (1982) popularized this Korcak law and pointed out that fractional Brownian motion will yield $B_T = D(P_T)/2$ = constant (= 1 - H/2). However, as discussed in detail in Lovejoy and Schertzer (1991) for multifractals, not only is B_T a function of T, but it has no special relation to $D(P_T)$.

PROPERTIES OF MULTIFRACTAL MEASURES

Multiplicative Processes and Topography

The general monofractal nature of processes produced by the addition of random noises and the general multifractal nature of the corresponding multiplicative processes have already been mentioned. The multiplicative processes that interest us here were first developed as models of turbulent cascades, initially proposed as a description of atmospheric

dynamics by Richardson (1922). There are now a whole series of such models: Novikov and Stewart (1964), Yaglom (1966), Mandelbrot (1974), Frisch et al. (1978), Schertzer and Lovejoy (1983, 1987), Benzi et al. (1984), and Meneveau and Sreenivasan (1987). In these models, the energy flux ε from large to small scales is conserved; hence, it is the basic cascade quantity. Directly observable fields such as the velocity shear (Δv_l) for two points separated by distance l are related to the energy flux through dimensional arguments:

$$\Delta v_l \approx \varepsilon_l^{1/3} l^{1/3} \tag{8.6}$$

The scaling $l^{1/3}$ can be viewed as a power-law filter ($k^{-1/3}$) in Fourier space (see the section on Nonstationary processes below). In contrast, the dynamical equations responsible for the topography are not known; the best we can do at present is to speculate on the fundamental dynamical quantities. In analogy with turbulence, we may expect the observable altitude fluctuations (Δh_l) to be related to a fundamental conserved quantity φ_l and the horizontal separation of the points as

$$\Delta h_l = \varphi_l^a l^H \tag{8.7}$$

Equation 8.7 indicates that the nonstationary topography process for altitude fluctuations Δh could be related to the underlying stationary φ. In the following, we show how a highly inhomogeneous multifractal topography will generically result if orographic processes are multiplicative and we outline some of their basic properties. Indeed, elsewhere (Lovejoy, et al., 1993) we show how equation 8.7 can be viewed as a multifractal general-

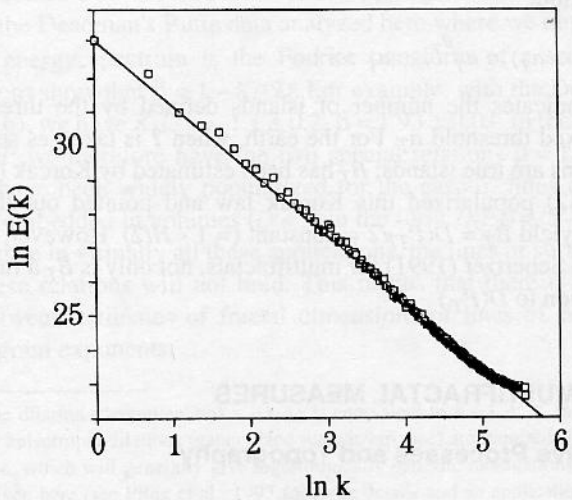

Figure 8.5 The spectral energy density as a function of the radial wave number for a grid mesh of 512 × 512, at 50-km resolution, of the Deadman's Butte data. The straight line is the best fit slope yielding exponent estimate $\beta \approx 1.93 \pm 0.03$.

ization of deterministic models of topography near ocean floor ridges, including a dimensional argument giving $H = 1/2$. Figure 8.6 illustrates an example of such a discrete multiplicative process for φ in two dimensions: a large structure of characteristic length l_0 with an initial uniform density φ_0 is broken up (via nonlinear interactions with other structures or through internal instability) into smaller substructures of characteristic length $l_1 = l_0/\lambda$ ($\lambda = 2$ is the scale ratio between two construction steps in this particular example), transferring in the process to each substructure a fraction of its density $\mu\varphi_0$. Figures 8.7 a–c show the analogous continuous cascade process for h, with the parameters corresponding to the topography as estimated below.

When the process is repeated, larger and larger values of φ appear, concentrated on smaller and smaller volumes; the result will be highly intermittent. Indeed, analysis shows that we obtain the following basic multifractal relations:

$$\varphi_\lambda \approx \lambda^\gamma, \quad \lambda > 1$$
$$Pr(\varphi_\lambda \geq \lambda^\gamma) \approx \lambda^{-c(\gamma)} \tag{8.8}$$

where φ_λ is the value of the multifractal at resolution λ, which is the ratio of the largest scale of interest to the smallest scale of the process. This indicates that the probability distribution of singularities of order higher than a value γ is related to the fraction of the space occupied by them, as determined by their codimension function $c(\gamma)$. Note that Equation 8.8 is nonlocal, that is, it is a relationship between the histograms of *incipient singularities* $\gamma_\lambda(\underline{x}) = \log \varphi_\lambda(\underline{x})/\log \lambda$ at different resolutions about the point $\underline{x}$ (it does *not* assume that a well defined limit exists at each point $\underline{x}$ when $\lambda \to \infty$), the singularities must be viewed as statistical exponents rather than point values.

Similarly, the qth order statistical moments of the field intensities will generally have a scaling exponent $K(q)$; using the definition for the statistical moments, we obtain the following relation:

$$\langle \varphi_\lambda^q \rangle \propto \lambda^{K(q)} \tag{8.9}$$

(In the limit $\lambda \to \infty$, the scaling exponents are related by the following Legendre transformations: $K(q) = \max_\gamma (q\gamma - c(\gamma))$; $c(\gamma) = \max_q (q\gamma - K(q))$. The turbulent notations $c(\gamma)$ and $K(q)$ are related to the more familiar strange attractor notation (Halsey et al., 1986) by the following: $\alpha_D = (D - \gamma)$, $f_D(\alpha_D) = D - c(\gamma)$, and $\tau_D(q) = (q - 1)D - K(q)$. We have added the subscript D to emphasize that the strange attractor notation fundamentally depends on the dimension of the observing space D; it cannot be used in stochastic processes where $D \to \infty$.

The multiplicative processes discussed above are quite general; however, various other (restrictive) types of multifractals exist. Table 8.1 gives a comparison of some of their properties. Up to now, most attention has been paid to the geometric multifractals (Parisi and Frisch, 1985; these very calm multifractals are defined purely geometrically

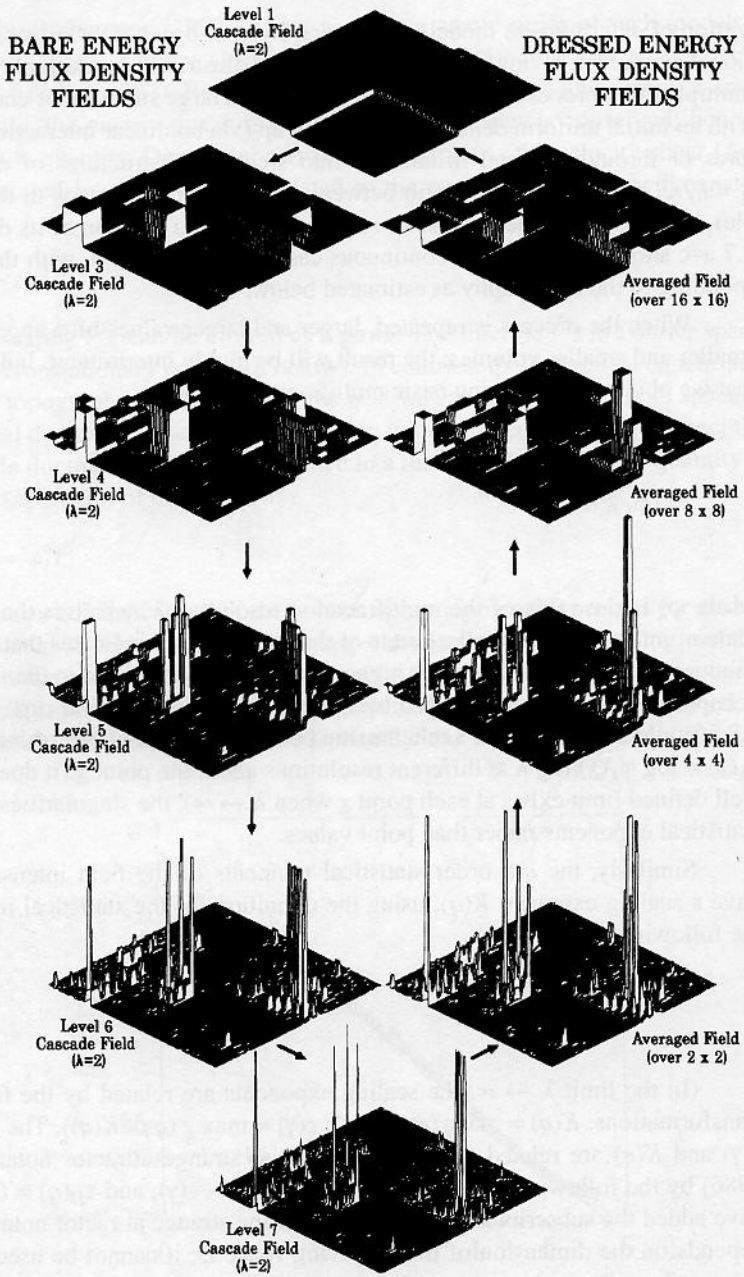

Figure 8.6 The left side shows the step by step construction of a "bare" multifractal process (the α model), starting with an initially uniform unit φ field. The vertical axis represents the density φ_λ flux to smaller scale with its ensemble average conserved ($<\varphi_\lambda> = 1$). At each step the horizontal scale is divided by 2. The developing spikes are incipient singularities of various orders (characteristic of multifractal processes). The right side shows the effect of smoothing over larger and larger scales, yielding the "dressed" quantities.

without any probability space) and to the "microcanonical" multifractals, which are also too calm for our present purposes.

Table 8.1 Classification of Multifractals According to Their Extreme Singularities

Type of Multifractal	Geometric	Microcanonical	Canonical
Types of singularities present	Calm	Calm	Calm, wild usually hard
Localized	Yes	No	No
Conservation per realization	Yes	Yes	No
Convergence of moments	All orders	All orders	Divergence of high orders

Figure 8.7 Three stages in the construction of a continuous multiplicative process for the topography field h, showing the effect of finer and finer resolution. The resolution increases from (a) 1/16th of the image size, to (b) 1/64th, to (c) 1/256th. This field is obtained by fractional integration of a continuous φ field, with parameters $H = 1/2$, $C_1 = 0.1$, and $\alpha = 1.8$.

Universal Multifractals

It has been shown that, for canonical processes, universality classes exist (for example, Schertzer and Lovejoy, 1987, 1988, 1989a; Schertzer et al., 1991; Wilson et al., 1991), which means that we may expect $K(q)$ to be given by the following functional form:

$$K(q) = \begin{cases} \dfrac{C_1}{\alpha - 1}(q^{\gamma} - q) & \alpha \neq 1 \\ C_1 q \log(q), & \alpha = 1, \quad \text{for } (\alpha < 2,\ q \geq 0) \end{cases} \tag{8.10}$$

where C_1 and α ($0 \leq \alpha \leq 2$) are the fundamental parameters needed to characterize the processes. The Lévy index α indicates the class to which the probability distribution belongs; it tells us how far we are from monofractality: $\alpha = 0$ corresponds to the monofractal β model; $\alpha = 2$ is the maximum. The above functions are for conserved (stationary) quantities and are the multiplicative analogs of the standard central limit theorem for the addi-

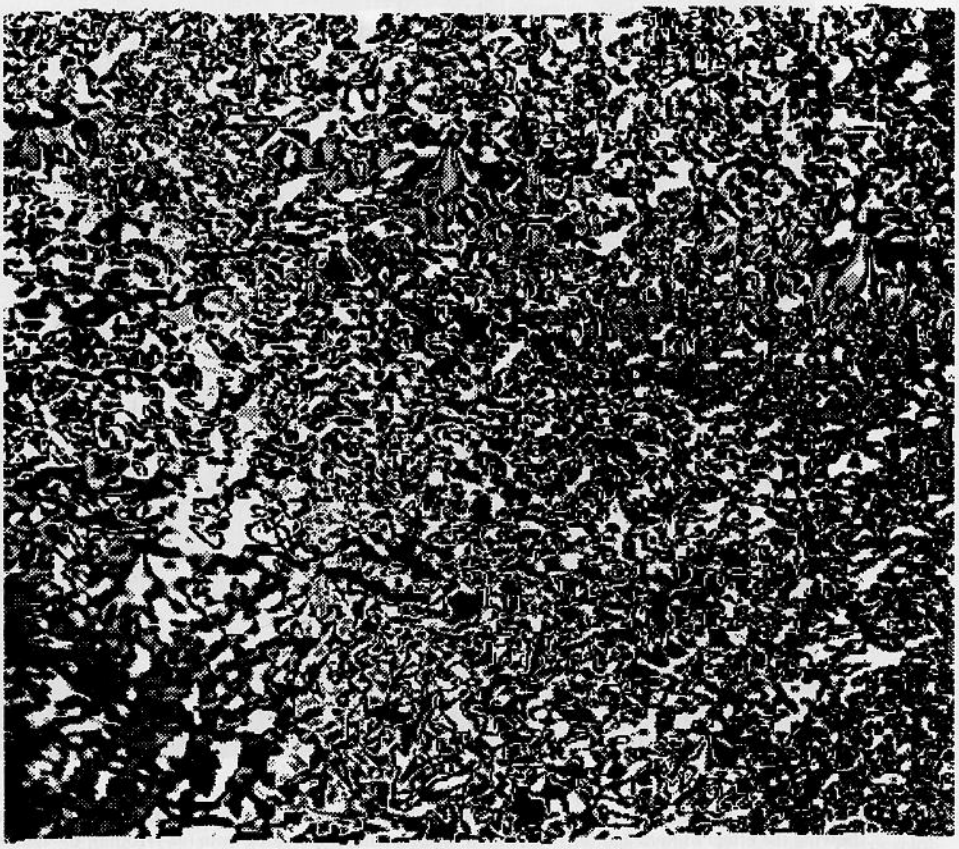

Figure 8.7(b)

tion of random variables. Closer analysis shows that there are actually five qualitatively different cases for the Lévy index α.

The case $\alpha = 2$ corresponds to log normal multifractals, $1 < \alpha < 2$ belongs to (log) Lévy processes with unbounded singularities, $\alpha = 1$ corresponds to log Cauchy multifractals, when $0 < \alpha < 1$ we have (log) Lévy processes with bounded singularities, and finally $\alpha = 0$ corresponds to the most popular and well-known monofractal β model (Novikov and Stewart, 1964; Mandelbrot, 1974; Frisch et al., 1978). A more detailed discussion of these fives cases and in particular of the generators of the Lévy variables can be found in Schertzer et al. (1988), Fan (1989), or Schertzer and Lovejoy (1989b).

The parameter C_1 is the fractal codimension of the singularities contributing to the average values of the field; it tells us about the sparsity of the average level of intensity. Furthermore, if $C_1 > D$ (the dimension of space in which the process is observed), then the multifractal is *degenerate* on the space; that is, it almost surely vanishes everywhere. When α is not much smaller than 2 (as in the topography data below), these are approximately lognormal, since with the exception of their extreme tails, these Lévy distributions

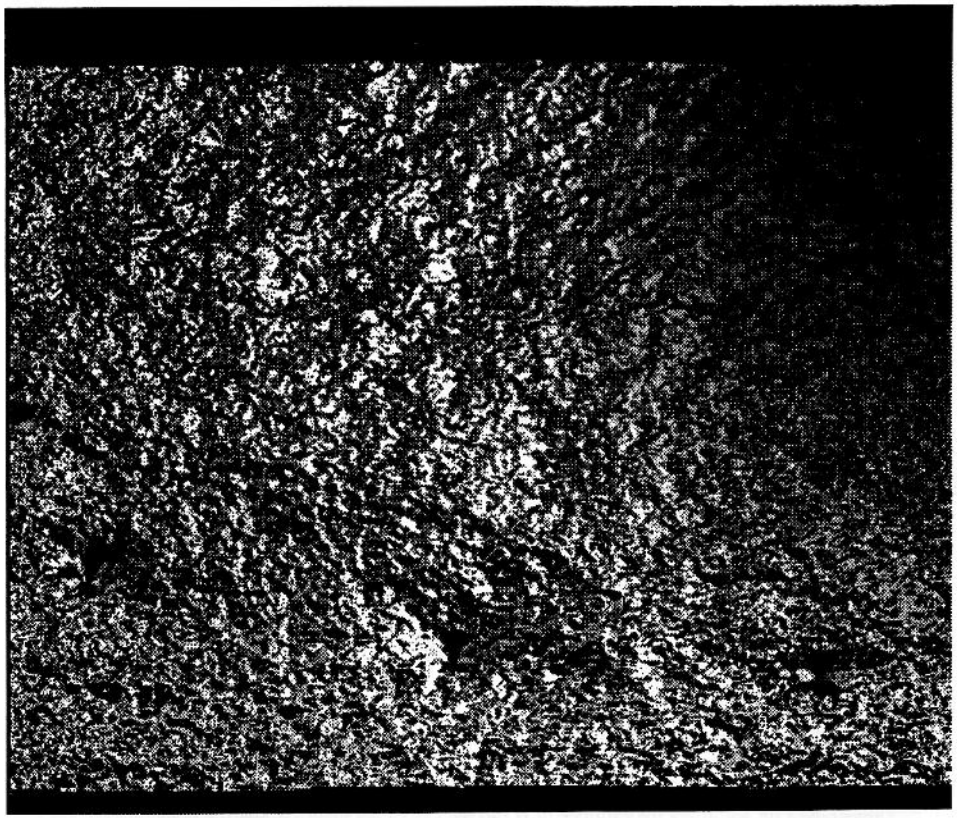

Figure 8.7(c)

are themselves nearly normal (this tail is pushed to lower and lower probability levels as $\alpha \rightarrow 2$). The widespread lognormal phenomeology is geophysics and geography is therefore an indication that the corresponding fields are actually multifractals, and are not exactly lognormal.

Nonstationary Processes

We have seen that in multiplicative processes there is always an underlying conserved quantity that has basic physical significance. In turbulence, it was the energy flux to smaller scales; in topography, it does not yet seem to be known, but we denoted it φ and related it to the altitude fluctuations via Equation 8.7. In terms of the scaling, conservation means $<\varphi_\lambda>$ = constant (independent of λ), hence $K(1) = 0$. If we consider the energy spectrum of φ_λ, it is $k^{-\beta}$ with $\beta = 1 - K(2)$; that is, the spectrum is always less steep than a $1/f$ noise.

If we consider the directly measurable altitude fluctuations Δh rather than φ, we find that $\Delta h_\lambda \approx \varphi_\lambda{}^a \lambda^{-H}$, where a is unknown (changing a is essentially the same as changing C_1; see below), and we anticipate that from the measurements below, $H = 1/2$ (if φ_λ was constant, then the altitude difference between two points would grow as the 1/2 power of their separation distance $\lambda^{-1/2}$). In Fourier space, the relation between $\varphi_\lambda{}^a$ and Δh_λ is simple: they will differ by k^{-H}; the spectra (the modulus squared of the Fourier transforms)

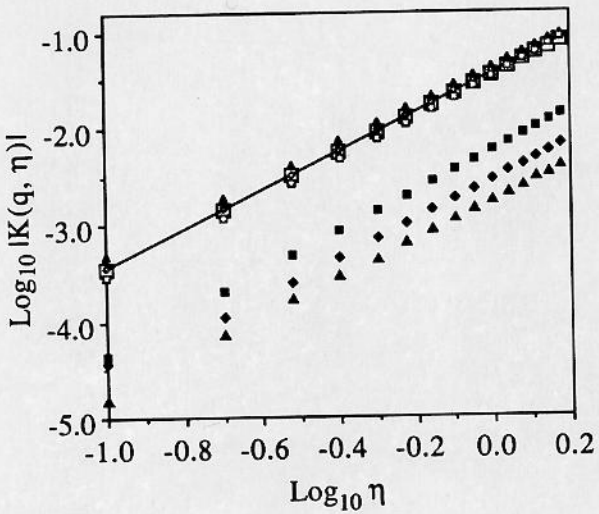

Figure 8.8. Log $|K(q, \eta)|$ versus log η, with $\alpha = 2$ (log normal), $C_1 = 0.15$, and $D = 2$, are given for $q = 0.5$. The curve of the stationary processes (big hollow square) is compared to those of the same processes after fractional differentiation (white symbols, $H = -2$, -1, and -0.5, from top to bottom). The fractional differentiation and integration do not affect the estimate of α (all the slopes are parallel), but fractional integration leads to biased estimates of C_1 (the curves with black symbols are all shifted downward compared to the theoretical stationary processes shown by the line).

will differ by k^{-2H}. Since (normal) differentiation of a function corresponds (ignoring constant factors) to multiplication by k in Fourier space and integration corresponds to division by k, we obtain the altitude fluctuations by the fractional integration (order H) of $\varphi_\lambda{}^a$. Conversely, if Δh_λ is measured, we may obtain φ_λ by fractional differentiation of the same order (see Schertzer and Lovejoy, 1991b, Appendix B.2, for more discussion of fractional derivatives and integrals).

The reason for dwelling on this is that it illustrates a basic point common to most geophysical fields, that their spectra have $\beta > 1$ and hence they cannot be stationary processes; they must be fractionally differentiated (that is, the spectra must be power law filtered) to become stationary. For topography, this means removing the λ^{-H} term and taking the a^{-1} power of the result in order to obtain the stationary φ from the nonstationary Δh_λ. The importance of this for standard data analysis has long been realized; for example, we have already seen that when $\beta > 1$ we should use variograms rather than autocorrelation functions [for example, analyze the differences (finite derivatives) of a time series rather than the series itself]. The same considerations apply to the use of the Double Trace Moment technique (below). Figure 8.8 shows the result when a simulated stationary process is fractionally integrated and differentiated by varying amounts: as long as we differentiate (filtered by k^H with $H > 0$), we obtain stable and accurate estimates of both C_1 and α; however, when we fractionally integrate ($H < 0$), we only recover α and C_1 is not accurately determined. Figure 8.8 also clearly indicates that, as long as the spectrum is less steep than the underlying stationary process [$\beta < 1 - K(2)$], we can recover C_1. After C_1, α are estimated, we can determine $K(2,1)$ from Equation 8.13 in the next section, and hence

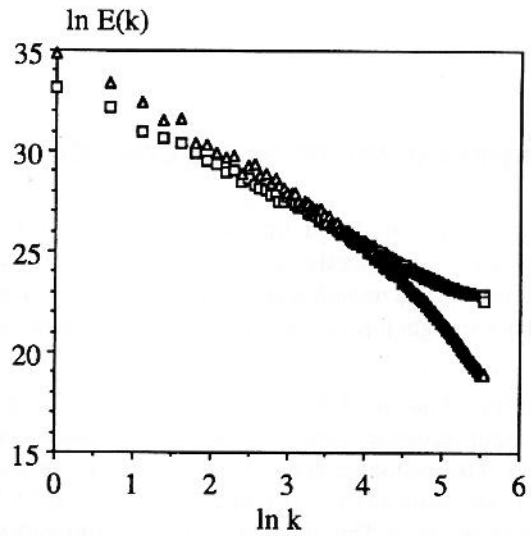

Figure 8.9 The spectrum of Deadman's Butte compared with the spectrum of the modulus of the gradient (which approximates a fractional differentiation of order 1), followed by a fractional integration of order 1. As expected, the curves are parallel for low frequencies, but at the high wave number end, they differ significantly over roughly the last factor 4.

the β of the stationary process, and infer the amount of fractional integration required to go from the underlying stationary process to the observed nonconserved process. Writing β for the spectral slope of the observed process, the order of fractional integration (the H in Equation 8.7) required to go from the stationary process to the nonstationary process is therefore given by

$$H = \frac{\beta - 1 + K(2)}{2} = \frac{\beta - 1}{2} + \frac{C_1 (2^{\alpha} - 2)}{2(\alpha - 1)} \tag{8.11}$$

This formula will be useful in the simulations described below where we produce multifractals with the same α, β, and C_1.

As a final comment before turning to the actual data analysis, we describe a shortcut that in many cases enables us to avoid the use of Fourier space. Recall that replacing the time series by its differences is essentially the same as multiplying by k in Fourier space. To generalize this to two (or more) dimensions, one possibility would be to use a finite difference Laplacian. This would multiply by $|\underline{k}|^2$ in Fourier space and hence the spectrum by $|\underline{k}|^4$; it would be quite drastic. We find that a compromise involving less smoothing that works quite well is to replace the field by the modulus of the local finite difference gradient operator. Figure 8.9 shows this explicitly on the height field data, which is discussed below. It compares the spectrum of the modulus of the gradient multiplied by k^{-1} in Fourier space with the spectrum of the original height field; the two curves are parallel as expected, except for high-wave-number deviations occurring roughly in the last factor of 4 of wave numbers. This deviation is not surprising: if a "cleaner" filtering is desired, Fourier methods should be used.

COMPARISON OF MONO AND MULTIFRACTAL EXPONENT RELATIONS

Now that we have introduced the essential difference between the nonstationary altitude h, and the stationary underlying flux φ, we summarize and compare their various properties in table 8.2.The monofractal limit ($\alpha \to 0$) is obtained when the convex curve of $K(q)$ becomes a straight line (a linear function of q). Simple scaling is the limit when $C_1 \to 0$ ($H \neq 0$).

The multifractal nature of the topography and the consequent failure of the equation $\beta = 2C(P_T) + 1$ can reconcile some of the apparently contradictory results summarized in Turcotte (1989). For example, using the value $\beta = 2$ for topography and the relation $\beta = 1 + 2C(P_T)$, we obtain $C(P_T) = 0.5$ and hence, $D(P_T) = 1.5$ for one dimensional cross-sections of the topography. This is in contradiction with various analyses of the lines of constant altitude (values of $D(P_T) \approx 1.2$–1.3 have often been reported.) However, as figure 1.1b shows, the value of $D(S \geq_T)$ (which is an upper bound for $D(P_T)$) is simply a function of altitude apparently tending to zero for large T; the discrepancy is simply a reflection of the multifractal nature of the topography.

Table 8.2 Summary of Various Scaling Exponents and the Simple Scaling Special Case

	General Multifractal/Multiscaling Result	Simple Scaling
Conserved flux scaling	$\langle \varphi_l^q \rangle = l^{-K(q)}$, $K(q)$ convex, $\neq 0$ [except $K(0)$, $K(1) = 0$]	$\langle \varphi_l^q \rangle$ independent of l, $K(q) = 0$
Altitude Structure function	$S_{q,l} = \langle \lvert \Delta h_l \rvert^q \rangle$; $K_h(q) = K(q) - qH$	$K_h(q) = -qH$
Spectral exponent	$\beta = 1 - K_h(2)$	$\beta = 1 + 2H = 1 + 2C(P_T)$
Codimension of exceedance sets $S \geq_T$	$C(S \geq_T)$ = increasing function of altitude threshold T	$C(S \geq_T) = 0$
Codimension of isolines P_T	$C(PT) \geq C(S_T \geq)$	$C(P_T) = H$ = constant
Exponent for the distribution of the area of islands	$B_T > 0$, function of T	$B_T = D(P_T)/2 = 1 - H/2$ = constant, independent of T

DOUBLE TRACE MOMENT ANALYSIS TECHNIQUE

When applied to turbulent and/or geophysical data (rather than to strange attractors), existing multifractal analysis techniques have had limited accuracy for a number of reasons. Techniques based on statistical moments (for example, partition function methods) suffer from both undersampling and divergence of moments, whereas others based on histograms or wavelets (with the exception of the probability distribution multiple scaling technique, Lavallée et al., 1991) assume that multifractals are local. Finally, these techniques have attempted to estimate an infinite number of parameters: the codimension function. We now describe a simple technique that overcomes these problems by exploiting the universality to estimate C_1 and α directly; $K(q)$ is then obtained using Equation 8.10 and $c(\gamma)$ by Legendre transformation of the same equation.

Consider the stationary multifractal process $\varphi_{\lambda'}(\langle \varphi_{\lambda'} \rangle = 1)$, where the resolution λ' is the ratio of the outer (or largest) scale of interest to the smallest scale of homogeneity. The basic idea is to generalize the application of statistical methods to the quantity $\varphi_{\lambda'}^{\eta}$, which is no longer conserved [$\langle \varphi_{\lambda'}^{\eta} \rangle = (\lambda')^{K(\eta)}$]. This is done by taking the η^{th} power of φ_{λ} at the largest scale ratio λ and then studying the scaling behavior of the various qth moments at decreasing values of the scale ratio $\lambda' \leq \lambda$. The q and η, double trace moments at resolution λ' and λ, have the following multiple scaling behavior (Lavallée, 1991; Lavallée et al., 1992):

$$\Pi_{\lambda'}^{(\eta)}(B_\lambda) = \int_{B_\lambda} \varphi_{\lambda'}^{\eta} d^D x \tag{8.12a}$$

$$Tr_{A_\lambda}(\varphi_{\lambda'}^{\eta})^q = \langle \sum_i \left[\Pi_{\lambda'}^{(\eta)}(B_{\lambda,i})\right]^q \rangle \approx \lambda^{K(q,\eta)-(q-1)D} \tag{8.12b}$$

where B_λ is a dimensional "ball" (square in figure 8.10), $\Pi_{\lambda'}^{(\eta)}(B_\lambda)$ is the "η flux" over the ball, and A_λ is the set A at resolution λ which results from covering the set with the balls (indexed with i). The sum is over all the balls in the covering. The integration over A_λ rescales the fields and "dresses" the quantities. When $\eta = 1$, the right side of Equation 8.12 reduces to the usual trace moments (which are themselves the ensemble average of the usual partition function).

The scaling exponent $K(q, \eta)$ is related to the usual $K(q) = K(q, 1)$ as follows (see Lavallée, 1991; Lavallée et al., 1992):

$$K(q, \eta) = K(q\eta, 1) - qK(\eta, 1) \tag{8.13}$$

$K(q, \eta)$ reduces to the usual $K(q, 1)$ when $\eta = 1$ and the right side of Equation 8.12b to the usual trace moments (Schertzer and Lovejoy, 1987, 1989a). The exponent $K(q,1)$ is the usual scaling exponent defined in Equation 8.10. Up to now it was written $K(q)$ for brevity and because no confusion was possible; for the rest of the paper, $K(q,1)$ will be used. Using Equation 8.10, the expression for $K(q, \eta)$ becomes

$$K(q, \eta) = \eta^{\alpha} K(q, 1) = \begin{cases} \dfrac{C_1}{\alpha - 1}\eta^a (q^a - q), & \alpha \neq 1 \\ C_1 \eta q \log(q) & \alpha = 1 \end{cases} \tag{8.14}$$

with $0 \leq \alpha \leq 2$, and $q \geq 0$ (for $\alpha \neq 2$).

Keeping q fixed (but different from the special values 0 or 1) and studying the scaling properties of the DTM for various values of η allows the determination of the scaling exponent $K(q,\eta)$ as functions of η and the slope of $|K(q, \eta)|$ as a function of η on a log–log graph, yielding a value of the parameter α. On the same log–log plot, the values of C_1 can be estimated by solving the expression for the intercept. For theoretical development and

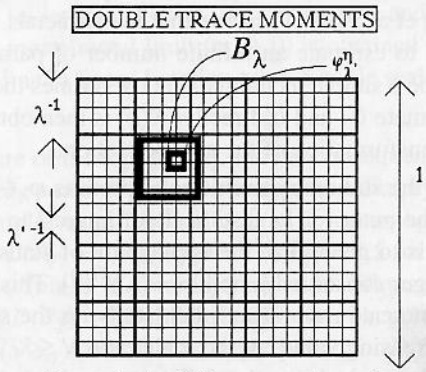

Figure 8.10 A schematic diagram illustrating the different averaging scales used in the double trace moments technique.

extensive numerical testing of the double trace moments technique, see Lavallée, 1991; Lavallée et al., 1992.

Equation 8.13 breaks down when $\max(q\eta, \eta) > \min(q_D, q_{\max})$ where q_D and $q_{\max}$ characterize, respectively, the divergence of moments and the undersampling (Lavallée et al., 1991a). In these cases, $K(q,1)$ becomes linear for q greater than these critical values, and Equation 8.13 indicates that scaling exponents $K(q, \eta)$ becomes independent of η.

EMPIRICAL RESULTS

The Universal Multifractal Parameters of Deadman's Butte

The DTM technique is now applied to the digital elevation model (DEM) of the Deadman's Butte region of Wyoming in the United States (see figure 8.17). The data were provided by P.J. Muller and D. Rees of University College, London. The height data, in meters, are distributed over a grid of 512 × 512 at 50-m resolution. As shown above, the spectral slope is $\beta \approx 1.93$ (Figure 8.5). Since $\beta > 1$, it is necessary to fractionally differentiate either in Fourier space or by studying the modulus of the gradient of the topography. Denoting the latter by $|\nabla h|$, we have

$$|\nabla h(x, y)| = \sqrt{\left(\frac{\partial h}{\partial x}\right)^2 + \left(\frac{\partial h}{\partial y}\right)^2} \tag{8.15}$$

which can be approximated by the following finite difference:

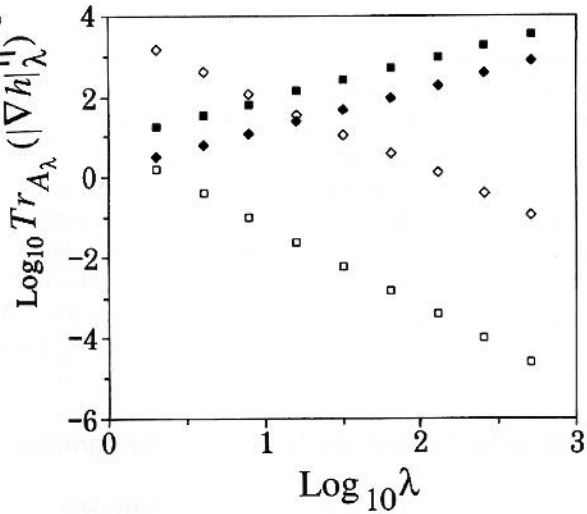

Figure 8.11 The scaling behavior of the double trace moments of the Deadman's Butte data is illustrated here by the straightness of the curves of the log $[Tr_{A\lambda}(|\nabla h|_\lambda^\eta)^q]$ as functions of the log(λ). The curves with positive slopes are those for $q = 0.5$, and from top to bottom $\eta = 2, 0.5$. The curves with negatives slopes are those for $q = 2$, and from top to bottom $\eta = 2, 0.5$. The slopes are $K(q, \eta)$ $(q - 1)D$.

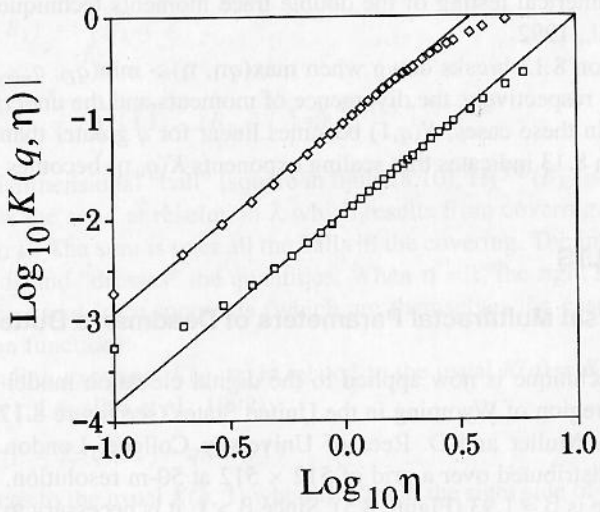

Figure 8.12 Log $|K(q, \eta)|$ versus log η for the Deadman's Butte data. [q is 2 (top) and 0.5 (bottom)]. All the curves are parallel as predicted by Equation 8.14. Their slopes, with $0.5 < \eta < 2.4$ are $\alpha \approx 1.90, 1.89$, and the corresponding C_1 are $\approx 0.044, 0.045$, respectively. The consistency between the estimates of α and C_1 for various values of q is a good indication that they are accurate. For values of η too high or too low, the curve $K(q, \eta)$ becomes fairly constant, as expected, and these values of log $|K(q, \eta)|$ must not be considered to estimate α.

$$|\nabla h(i,j)| = \sqrt{[h(i+1,j) - h(i-1,j)]^2 + [h(i,j+1) - h(i,j-1)]^2} \tag{8.16}$$

where $\Delta x = \Delta y = 1$. The indexes i and j are, respectively, the horizontal and vertical coordinates, in our case going both from 1 to 512. The difference operations are applied without privileging any particular direction; problems related to anisotropy are neglected. The field $|\nabla h|$ is raised to the power η at its smallest scale length, and the qth statistical trace moment of the field is estimated from $\lambda = \lambda' = 2^9 = 512$ to $\lambda = 2$. The rescaled field intensities are obtained by averaging over the $|\nabla h|^\eta$ at the finest resolution.

The scaling behavior of the log $[Tr_{A\lambda}(|\nabla h|_\lambda^\eta)^q]$ against log(λ) is given in Figure 8.11 for several values of q and η. The slopes of these curves give the estimated scaling exponents $K(q, \eta)$. Log $[|K(q, \eta)|]$ as a function of log η is shown in Figure 8.12. From this curve, the estimated parameters are $C_1 \approx 0.045 \pm 0.005$ and $\alpha = 1.9 \pm 0.1$. Finally, using our estimate $\beta = 1.93$, we can use Equation 8.11 to estimate the parameter $H = (1.93 - 1)/2 + 0.045(2^{1.9} - 2)/(2 \times 0.9) \approx 0.51 \approx 1/2$.

Universal Multifractal Parameters for French Topography

For comparison with the 50-m resolution Deadman's Butte data, we also applied the DTM technique to a DEM of French topography of 512 × 512 pixel at 1-km resolution. Figure 8.13 shows various DTM as functions of the resolution, indicating the accuracy with which the scaling is respected when λ varies from 2^9 to 2, and Figure 8.14 shows the curves log $K(q, \eta)$ against log η, indicating that over the range $0.01 < \eta < 3$ universality

holds very well. As expected at both large and small η, the small sample size (a single realization) leads to serious sampling problems for these extreme moments. For $q = 0.5$, 2, 4, we have very parallel lines with slopes very near $\alpha = 1.7$; analysis of the intercepts with $\log \eta = 0$ indicates that $C_1 = 0.075 \pm 0.005$. These values should be compared with the values for Deadman's Butte ($\alpha = 1.9$, $C_1 = 0.045 \pm 0.005$), recalling that these are statistical exponents and that single realizations of multifractal processes will be extremely variable. To compare the two $K(q, \eta)$ functions, we plot (Figure 8.15) for $q = 2$ and show the intermediate slope $\alpha = 1.8$ for reference. Although we can be quite confident that the values of C_1 of the corresponding multifractal processes really are different, the values of the more fundamental multifractal index α may in both cases be compatible with the common value $\alpha = 1.8$, although many more data sets will need to be analyzed to be sure.

Discussion

The obtained values of H, C_1, and α indicate that the height field has seemingly paradoxical properties that go a long way toward explaining both the successes and the limitations of monofractal analyses and models. First, the multifractal index α is nearly its maximum, indicating that singularities of all orders contribute significantly to the process: we are almost as far as possible from the monofractal case $\alpha = 0$. However, the modest values of C_1 indicate that the mean of φ is not too sparse (a space-filling mean would have $C_1 = 0$). Due to the fractional integration ($H = 1/2$) necessary to obtain the height field from φ, even if $C_1 = 0$, we would still obtain a fractal height field; however, its properties would be independent of the altitude and yield fractal dimensions $2 - H = 1.5$ for lines of constant

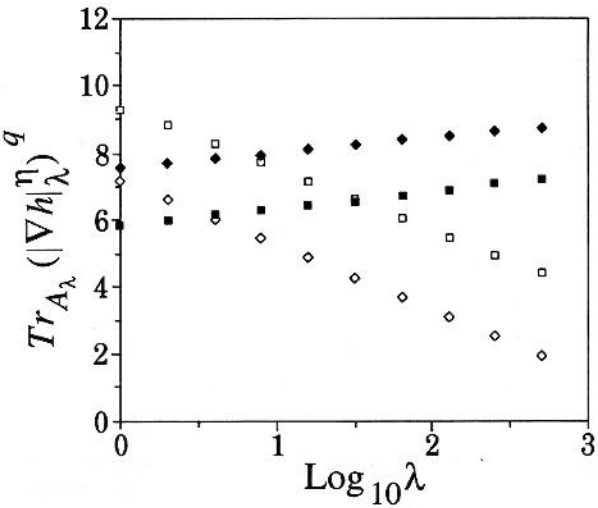

Figure 8.13 Same as Figure 8.11 but for the French topography; when $q = 0.5$ (curves with a positive slope), $\eta = 2.26$, 0.56 from top to bottom; when $q = 2$ (curves with a negative slope), $\eta = 1.6$, 0.56 from top to bottom.

altitude. Hence, our value of C_1 is in perfect accord with the standard empirical results for those statistics which do not depend sensitively on the extremes. However, once we start examining isolines at high altitude or high-order moments, the large value of α will ensure that the multifractal nature of the process will be important.

Actually, the low values estimated for C_1 in both cases may not be very significant because (as mentioned in the section on the DTM technique) the DTM technique cannot distinguish between the conserved process φ and an arbitrary power a of the process. In other words, the fundamental conserved process responsible for topography could have significantly larger $C_1 a^{\alpha}$. Indeed, this is exactly the case for the velocity and temperature fields analyzed in Schmitt et al. (1992a and b), where the value $a = 3$ is determined by dimensional arguments and low values ($\approx$0.1) for the C_1 of the velocity field are associated with significantly larger values ($\approx$0.25) for the underlying energy flux ε.

Numerical Simulations of Isotropic, Self-similar Universal Topography

As explained earlier, universal multifractals arise when scaling multiplicative processes are mixed: either by nonlinear interactions between different processes or by nonlinear interactions between structures at intermediate scales (that is, a *densification* of the cascade leading to a continuous cascade). Because of the existence of stable, attractive universal multifractal generators, the results of such processes are independent of most of the details; hence, we may expect to observe universal multifractals in many diverse areas

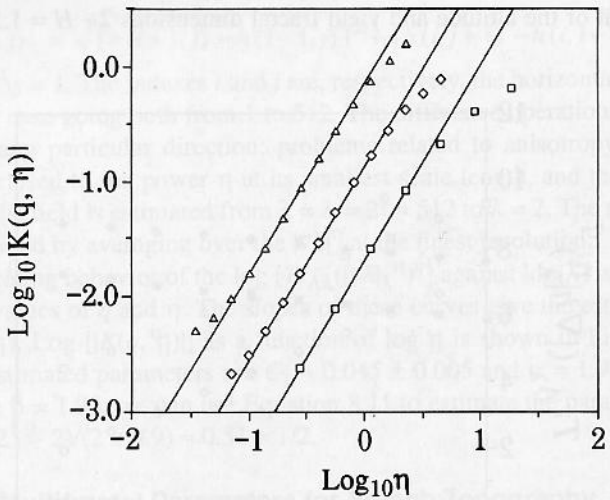

Figure 8.14 Same as Figure 8.12 for the French topography. From top to bottom, q takes the following values: 4, 2, and 0.5. The estimates of the slope for $q = 4$, with η taking values between 0.1 and 0.5, give $\alpha = 1.67$. The same analysis for $q = 2$ and 0.5 (with η taking values between 0.12 and 1.1 in the first case and between 0.3 and 2.3 in the second) yields respectively, $\alpha = 1.69$, 1.7. The values of C_1, obtained by solving the expression for the log $\eta = 0$ intercept given by the log $|K(q, 1)|$ and using Equation 8.10, are, respectively; 0.0078, 0.076, and 0.076. Here also the values of α, C_1 determined are independent of the q values.

where the dynamics are strongly nonlinear and occur over wide ranges of scale. In turbulence, the physical basis of these universal multifractals is the scaling symmetry, conservation of energy flux, and cascading phenomena, which implies that the dynamics at one scale mainly modulate the nearby scales. In topography and most other geophysical and geographical fields, the exact dynamical equations and the corresponding conserved areas of statistics are usually not known. However, just as Gaussian distributions occur in many areas of statistics, so we may expect universal multifractals to arise in many scaling nonlinear dynamical systems. Indeed, the prevalence of nearly log normal phenomena in geography and geophysics suggests the ubiquity of multifractals.

Wilson et al. (1991) describe the numerical simulation of clouds and topography, including how to iteratively zoom in and calculate details to arbitrary resolution in selected regions. Although we will not repeat these details here, enough information has been given in the previous sections to understand how they work. First, recall that a conserved (stationary) multifractal process φ_λ has a generator $\Gamma_\lambda = \log \varphi_\lambda$, which is exactly a $1/f$ noise; that is, its spectrum is $E(k) \approx k^{-1}$ (this is sufficient to ensure the multiple scaling of the moments of φ_λ). Therefore, to produce a generator, we start with a stationary Gaussian or Lévy *subgenerator*. The subgenerator is a noise consisting of independent random variables with either Gaussian ($\alpha = 2$) or extreme Lévy distributions (characterized by the Lévy index α), whose amplitude (for example, variance in the Gaussian case) is determined by C_1. The subgenerator is then fractionally integrated to give a k^{-1} spectrum. This generator is then exponentiated to give the conserved φ_λ, which will thus depend on both C_1 and α. Finally, to obtain a nonconserved process with spectral slope β, the result is fractionally integrated by multiplying the Fourier transform by k^{-H} where H is given in Equation 8.11. The entire process involves two fractional integrations and hence four FFTs. Fields of 512×512 can easily be modeled on personal computers (they take about 3

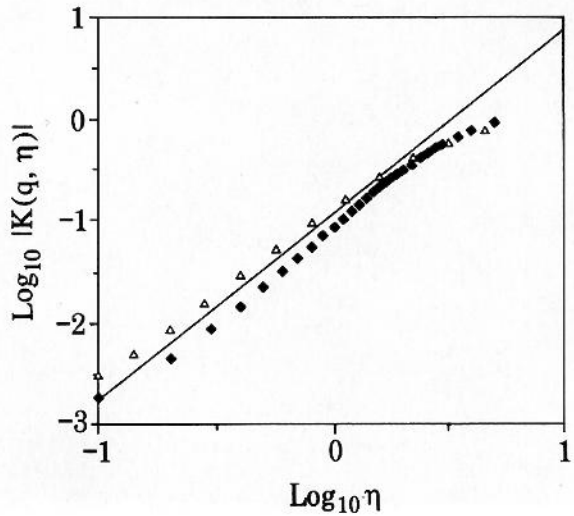

Figure 8.15 Log $|K(q, \eta)|$ for the French topography (top) and Deadman's Butte (bottom) are compared with $q = 2$. The lines have slopes equal to 1.8.

minutes on a Mac II), and 256 × 256 × 256 fields, for example, for the temporal evolution of clouds, have been produced on a Cray 2. Such cloud simulations have been turned into a video called *multifractal dynamics* (Brenier, 1990; Brenier et al., 1990).

Figures 8.7a–c show the results for parameters similar to those found for Deadman's Butte and France. Another example with $\alpha = 1.6$ (Figure 8.16) is shown to indicate the range of behavior achieved by varying the multifractal index α. The commonly used ray-tracing technique has been used to visualize the simulations since this effectively highlights the surface texture. Perhaps one of the most striking differences between the figures is the existence of smooth low "plains" when $\alpha < 2$ (most visible for $\alpha \approx 1.6$), which is a direct consequence of the extremal Lévy character of the random variables used in the corresponding generator. In effect, when $\alpha < 2$, there must be a more and more marked asymmetry between positive and negative fluctuations in the generator: the negative fluctuations becoming more and more extreme with respect to the positive ones as α decreases. When the generator is exponentiated to give the conserved process, the result is strong *holes*, some of which can be large, in which the conserved process will nearly vanish. Finally, the power-law filter (k^{-H}) applied to generate the topography field is a smooth-

Figure 8.16 Simulation of topography with multiplicative cascade processes visualized using ray tracing techniques, with $\alpha = 1.6$, $C_1 = 0.1$, and $H = 1/2$.

ing operation that tends to round out the holes somewhat; nevertheless, their effect is clearly visible in the simulations.

Figure 8.17 shows the Deadman's Butte data with the same format. The most obvious visual difference between this and the preceding simulations is that the Butte data have far more interesting texture due to their anisotropy, which is present at all length scales. Clearly, more realistic topography models will have to go beyond the restrictive isotropic (self-similar) framework described here. Following the formalism of generalized scale invariance (mentioned earlier), this will require introducing a new generator for the scale-changing operations.

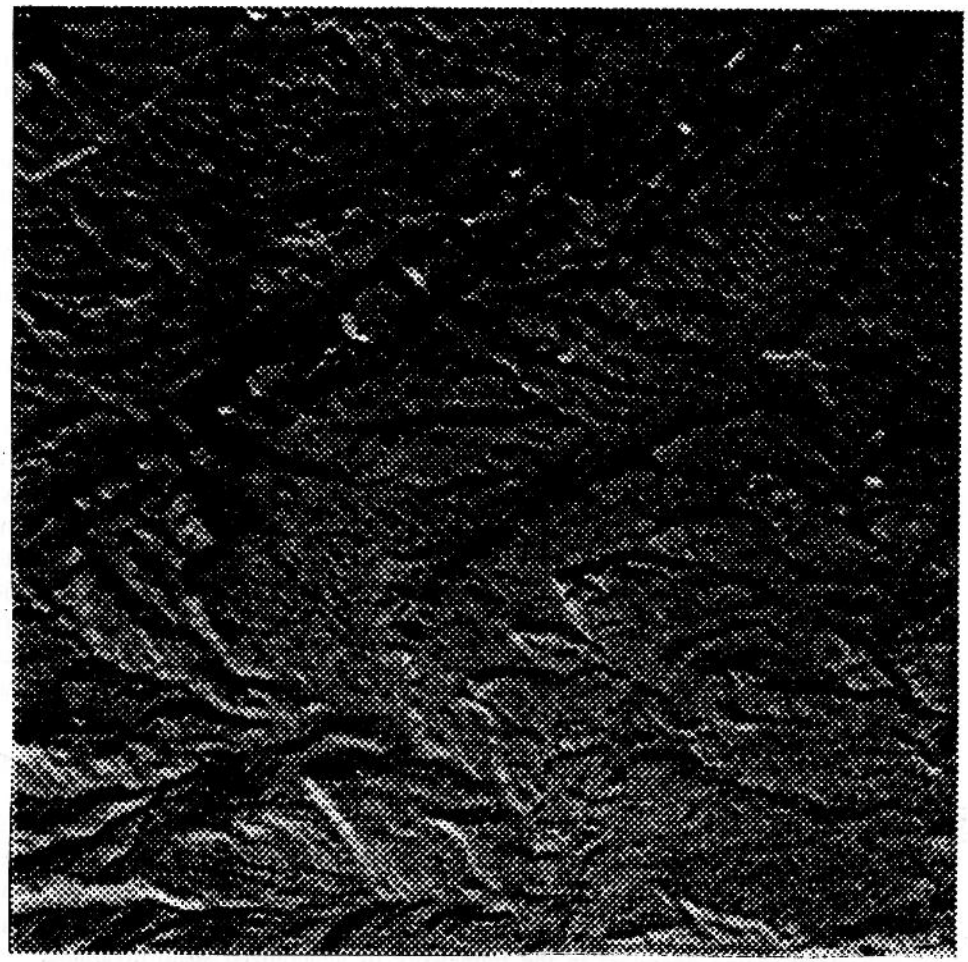

Figure 8.17 The topography of Deadman's Butte shown with ray tracing techniques.

CONCLUSION

The problem of adequately conceptualizing and modeling the extremely variable geophysical and geographical fields in our environment has a long history. Of the various ideas that have been put forward to deal with the problem, the notion of scale invariance is undoubtedly the most seductive because it is the simplest hypothesis that seems to be capable of accounting for the ubiquity of complex geographical fields spanning many orders of magnitude in scale.

Early ideas of scaling involved restrictive scale-changing operations: structures were assumed statistically isotropic (self-similar). This means that they were unable to deal with differential rotation, compression, or texture. Furthermore, restrictive types of scaling appropriate for fractal sets, but not for multifractal fields, were used. In the first part of this paper, we reviewed these issues, demonstrating explicitly how many commonly used methods for estimating fractal dimensions (such as spectral or variogram–structure function exponents) can only be used for dimension estimates in monofractal systems.

We continued our review with an outline of multiplicative processes, indicating briefly how they lead to universal multifractals when they are mixed. Stable and attractive generators of multiplicative processes exist, and they are likely to arise from diverse nonlinear mechanisms; the details are unimportant in the limit where interactions between many different processes occur or where interactions occur over a continuum of length scales.

We then outlined the new double trace moments analysis technique, which is the first to be specifically designed to estimate the universal multifractal indexes and tested it on multifractal simulations. We applied this technique to digital elevation models of Deadman's Butte (50-m resolution) and French topography (1-km resolution), obtaining the estimates $\alpha = 1.9 \pm 0.1$ and $\alpha = 1.7 \pm 0.1$, respectively, for the multifractal indexes, and $C_1 = 0.045 \pm 0.005$ and $C_1 = 0.075 \pm 0.005$ for the codimension of the mean of the corresponding conserved process. The multiple scaling of the data sets was accurately confirmed over the entire range of scale (factor 512 in both cases), and the universality of the scaling exponents over the range 0.1 to 3 is identified. For exponents larger than this, we have an undersampling problem: many realizations must be used to get more accurate estimates for these extreme exponents, for exponents smaller than this the results are dominated by noise or measurement errors.

Finally, we briefly described how to simulate such fields and produce simulations with the same α, C_1, and spectral exponents β (≈ 2 here). We argue that the fundamental difference between the simulations and the data is that the former are constructed to be isotropic (self-similar), whereas the latter are highly anisotropic. More realistic models can easily introduce scaling anisotropy (including stochastic anisotropy to deal with locally varying differential compression and rotation of structures) by using anisotropic scale-changing operators in the framework of generalized scale invariance (GSI) (see Lovejoy et al., 1992; Pflug et al., 1993). This is the current subject of empirical, numerical, and theoretical investigation.

ACKNOWLEDGEMENTS

We thank A. Davis, C. Hooge, K. Pflug, F. Schmitt, Y. Tessier, and B. Watson for helpful comments, discussion, and technical assistance. G. Sarma is thanked for the simulation and D. Rees and J. P. Muller for the Deadman's Butte DEM data and for helpful criticism.

REFERENCES

Aviles, C. A., Scholz, C. H., and Boatwright, J. 1987. Fractal analysis applied to characteristic segments of the San Andreas Fault. *Journal of Geophysical Research* 92:331–334.

Bell, T. H. 1975. Statistical features of sea floor topography. *Deep Sea Research* 22:883–891.

Benzi, R., et al., 1984. On the multifractal nature of fully developed turbulence and chaotic systems. *Journal of Physics A* 17:3521–3531.

Bills, B. G., and Kobrick, M. 1985. Venus topography: A harmonic analysis. *Journal of Geophysical Research* 90:827–836.

Brenier, P. 1990. Simulations du dynamique multifractal des nuages. Master's Thesis, Ecole Normale du Science et Technologie Avancée. Paris, France.

———, et al. 1990. Continuous multiplicative cascade models of passive scalar clouds. *Annales Geophysicae* 8, Special Issue: 320.

Clarke, K.C. 1988. Scale-based simulation of topographic relief. *The American Cartographer* 15: 173–181.

De Cola, L. 1989. Multiscale data models for spatial analysis, with applications to multifractal phenomena. In *Proceedings, Ninth International Symposium on Computer-assisted Cartography (Auto-Carto 9)*, Baltimore, pp. 313–323.

———. 1990. Fractal analysis of a classified Landsat scene. *Photogrammetric Engineering and Remote Sensing* 55(5):601–610.

Falconer, K. 1990. *Fractal Geometry: Mathematical Foundations and Applications*. New York: J. Wiley and Sons.

Fan, A. H. 1989. Chaos additif et multiplicatif de Lévy. *Comptes Rendus. Academie des Sciences (Paris) I* 308:151–154.

Fournier, A., Fussell, D., and Carpenter, L. 1982. Computer rendering of stochastic models. *Communications of the Association of Computing Machinery* 6:371–374.

Fox, C. G. 1989. Empirically derived relationships between fractal dimension and power law from frequency spectra. *Pure and Applied Geophysics* 131:211–239.

Frisch, U., Sulem, P. L., and Nelkin, M. 1978. A simple dynamical model of intermittency in fully developed turbulence. *Journal of Fluid Mechanics* 87:719–724.

Gabriel, P., et al., 1988. Multifractal analysis of resolution dependence in satellite imagery. *Geophysical Research Letters* 15:1373–1376.

Gilbert, L. E. 1989. Are topographic data sets fractal? *Pure and Applied Geophysics* 131:241–254.

Goodchild, M. F. 1980. Fractals and the accuracy of geographical measures. *Mathematical Geology* 12:85–98.

Halsey, et al., 1986. Fractal measures and their singularities: the characterization of strange sets. *Physics Review A* 33:1141-1151.

Klinkenberg, B., and Clarke, K.C. 1992. Exploring the fractal mountains. In *Automated Pattern Analysis in Petroleum Exploration*, I. Palaz, and S. Sengupta, eds., pp 261–212. New York: Springer-Verlag.

———, and Goodchild, M. G. 1992. The fractal properties of topography: A comparison of methods. *Earth Surficial Processes and Landforms* 17: 217–234

Kolmogorov, A. N., 1940. Wienersche spiralen and einige andere interessante kurven in Hilbertschen Raum. *C. R. (Doklady) Acad. Sci. URSS (N.S.)* 26: 115–118.

———, and Tihomirov, V. M. 1959. Epsilon entropy and epsilon capacity of sets in functional spaces. *Uspeckhi Matematicheskihk Nauk (N.S.)* 14:3–86. Translated in *American Mathematical Society Translations (Series 2)* 17:277–364.

Korcak, J. 1938. Deux types fondamentaux de distribution statistique. *Bulletin de l'Institut International de Statistique* III: 295–299.

Ladoy, P., Schertzer, D., and Lovejoy, S. 1990. Analyse multifractale du relief Français. Manuscript.

Lamperti, J. 1962. Semi-stable stochastic processes. *Transactions, American Mathematics Association* 204: 62–78.

Lavellée, D. 1991. Multifractal techniques: Analysis and simulations of turbulents fields. Ph.D. Thesis, McGill University, Montréal, Canada.

———, Schertzer, D., and Lovejoy, S. 1991. On the determination of the codimension function. In *Non-linear Variability in Geophysics: Scaling and Fractals*, D. Schertzer, and S. Lovejoy, eds. Dordrecht, the Netherlands: Kluwer.

———, ———, ———, and Schmitt, F. 1992. On the determination of universal multifractal parameters in turbulence. In *Topological aspects of the dynamics of fluids and plasmas*. H. K. Moffal, et al., eds., pp. 463–478. Dordrecht-Boston: Kluwer.

Lovejoy, S., Schertzer. D., and Tsonis, A. A. 1987: Funcional box counting and multiple elliptical dimensions in rain, *Science, 235*, 1036–1038

———, and ———. 1988a. Extreme variability, scaling and fractals in remote sensing: Analysis and simulation. In *Digital Image Processing in Remote Sensing*, J. P. Muller, ed., pp. 177–212. London: Taylor & Francis.

———, and ———. 1988b. Meeting report: Scaling, fractals, and non-linear variability in geophysics. *EOS* 69:143–145.

———, and ———. 1990a. Our multifractal atmosphere: A unique laboratory for nonlinear dynamics. *Physics in Canada* 46:62–71.

———, and ———. 1990b. Multifractals, universality classes and satellite and radar measurements of cloud and rain fields. *Journal of Geophysical Research* 95:2021–2034.

———, and ———. 1991. Multifractal analysis techniques and the rain and cloud fields from 10^{-3} to 10^{-6} m. In *Non-linear Variability in Geophysics: Scaling and Fractals*, D. Schertzer and S. Lovejoy, eds., pp. 111–144. Dordrecht, The Netherlands: Kluwer.

———, ———, and Ladoy, P. 1986a. Fractal characterization of inhomogeneous measuring networks, *Nature* 319:43–44.

———, ———, and ———. 1986b. Brighter outlook for weather forecasts. *Nature* 320:401.

———, ———, and Pflug, K. 1992. Generalized scale invariance and differential rotation if cloud radiances. *Physica A* 185: 121–128.

———, Lavallée, D., Schertzer, D., and Ladoy, Pl 1993. Topography as a universal multifractal process and the $l^{1/2}$ law. Manuscript.

Mandelbrot, B. 1975. Stochastic models for the earth's relief, the shape and the fractal dimension of the coastlines and the number-area rule for islands. *Proceedings of the National Academy of Sciences, USA* 72:3825–3828.

———. 1967. How long is the coastline of Britain? Statistical self-similarity and fractional dimension. *Science* 155:636–638.

———. 1974. Intermittent turbulence in self-similar cascades: Divergence of high moments and dimensions of the carrier. *Journal of Fluid Mechanics* 62:331–358.

———. 1977. *Fractals—Form, Chance and Dimension*. San Francisco: W. H. Freeman & Co.

———. 1982. *The Fractal Geometry of Nature*. San Francisco: W. H. Freeman & Co.

———, and Van Ness, W. 1968. Fractional Brownian motions, fractional noises and applications. *SIAM Review* 10: 422–450.

Mareschal, J. C. 1989. Fractal reconstruction of sea-floor topography. *Pure and Applied Geophysics* 131:197–210.

Mark, D. M., and Aronson, P. B. 1984. Scale dependent fractal dimensions of topographic surfaces: An empirical investigation, with applications in geomorphology and computer mapping. *Mathematical Geology* 16:671–683.

Meneveau, C., and Sreenivasan, K. R. 1987. Simple multifractal cascade model for fully developed turbulence. *Physical Review Letters* 59(13):1424–1427.

Novikov, E. A., and Stewart, R. 1964. Intermittency of turbulence and spectrum of fluctuations in energy-dissipation. *Izvestiya Akademii Nauk SSSR Serija Geofizicheskaya [USSR]* 3:408–412.

Okubo, P. G., and Aki, A. 1987. Fractal geometry in the San Andreas fault system. *Journal of Geophysical Research* 92:345–355.

Parisi, G., and Frisch, U. 1985. A multifractal model of intermittency. In *Turbulence and Predictability in Geophysical Fluid Dynamics and Climate Dynamics*, M. Ghil, R. Benzi, and G. Parisi, eds., pp. 84–88. Amsterdam: North-Holland.

Perrin, J. 1913. *Les Atomes*. Paris: NRF-Gallimard.

Pflug, L. Lovejoy, S. and Schertzer, D. 1993. Differential rotation and cloud testure: analysis using generalized scale invariance. *Journal of Atmospheric Science* 50:538–553.

Rees, D., and Muller, J. P. 1990. Anomalies resulting from the characterization of terrain by fractional Brownian motion. Manuscript.

Richardson, L. F. 1922. (Republished by Dover, New York, 1965). *Weather Prediction by Numerical Process*. London: Cambridge University Press.

———. 1961. The problem of contiguity: An appendix of statistics of deadly quarrels. *General Systems Yearbook* 6:139–187.

Sarma, et al. 1990. Universal multifractal cascade models of rain and clouds. Preprint vol., American Meteorological Society Conference on Cloud Physics, San Francisco, July 24–27, pp. 255–262.

Schertzer, D., and Lovejoy, S. 1983. Elliptical turbulence in the atmosphere. Proceedings of the *4th Symposium on Turbulent Shear Flows* 11.1–11.8, Karlsrhule, Germany.

——— and ———. 1985. Generalized scale invariance in turbulent phenomena. *Physico-Chemical Hydrodynamics Journal* 6:623–635.

——— and ———. 1987. Physically based rain and cloud modeling by anisotropic, multiplicative turbulent cascades. *Journal of Geophysical Research* 92: 9693–9714.

——— and ———, et al., 1988. Universal multifractals in turbulence. In *Fractal Aspects of Materials: Disordered Systems*, D. A. Weitz, L. M. Sander, and B. B. Mandelbrot, eds., pp. 267–269. Pittsburg, PA: Materials Research Society.

——— and ———. 1988. Multifractal simulations and analysis of clouds by multiplicative processes. *Atmospheric Research* 21:337–361.

——— and ———. 1989a. Nonlinear variability in geophysics: multifractal analysis and simulations. In *Fractals: Their Physical Origins and Properties*, L. Pietronero, ed., pp. 49–79. New York: Plenum Press.

——— and ———. 1989b. Generalized scale invariance and multiplicative processes in the atmosphere *Pure and Applied Geophysics* 130:57–81.

——— and ———. 1991a. Preface. In *Non-linear Variability in Geophysics: Scaling and Fractals*, D. Schertzer, and S. Lovejoy, eds., pp. vii–ix. Dordrecht, The Netherlands: Kluwer.

——— and ———. 1991b. Nonlinear geodynamical variability: Multiple singularities, universality and observables. In *Non-linear Variability in Geophysics: Scaling and Fractals*, D. Schertzer, and S. Lovejoy, eds., pp. 41–82. Dordrecht, The Netherlands: Kluwer.

——— and ———. 1992. Hard and soft multifractal processes. *Physica A* 185: 187–194.

——— et al. 1991. Universal hard multifractal turbulence: Theory and observations. In *Nonlinear Dynamics of Structures*, R. Z. Sagdeev, et al., eds., pp. 213–236, Teaneck, New Jersey: World Scientific.

Schmitt, F., et al. 1992a. Estimates of Universal multifractal indices for velocity and temperature fields. *Comptes Rendus. Academie des Sciences (Paris), II-56*: 749–754.

———, ———. 1992a. Empirical determination of universal multifractal exponents in turbulent velocity fields, Physical Review Letters 68: 305–308.

Steinhaus, H. 1954. Length, shape and area. *Colloquium Mathematicum* 3:1–13.

———. 1962. *Mathématiques en instantanés*. Paris: Flammorion.

Tessier, Y., Lovejoy, S. and Schertzer. D. 1993. Universal Multifractals: Theory and observations for rain and clouds. *Journal of Applied Meteorology* 32:223–250.

Turcotte, D. L. 1989. Fractals in geology and geophysics. *Pure and Applied Geophysics* 131:171–196.

Venig-Meinesz, F. A. 1951. A remarkable feature of the Earth's topography. *Proceedings, Koninklijke Nederlandse Akademie Van Wetenschappen. Series B. Physical Sciences* 54:212–228.

Voss, R. F. 1983. Fourier synthesis of Gaussian fields: 1/f noises, landscapes and flakes. Preprints, Siggraph Conference, Detroit, 21 pp.

Wilson, J., Schertzer, D., and Lovejoy, S. 1991. Physically based cloud modeling by multiplicative cascade processes. In *Non-linear Variability in Geophysics: Scaling and Fractals*, D. Schertzer, and S. Lovejoy, eds., Dordrecht, The Netherlands: Kluwer.

Yaglom, A. M. 1966. The influence of the fluctuation in energy dissipation on the shape of turbulent characteristics in the inertial interval, *Soviet Physic. Doklady* 2:26–30.